Vision-based Control of 2D Plane Poiseuille Flow

R. Tatsambon Fomena, Christophe Collewet

▶ To cite this version:

R. Tatsambon Fomena, Christophe Collewet. Vision-based Control of 2D Plane Poiseuille Flow. 7th Int. Symp. on Turbulence and Shear Flow Phenomena, Jul 2011, Ottawa, Canada. inria-00629708

HAL Id: inria-00629708
https://hal.inria.fr/inria-00629708

Submitted on 6 Oct 2011

VISION-BASED CONTROL OF 2D PLANE POISEUILLE FLOW

Romeo Tatsambon Fomena and Christophe Collewet

Cemagref, INRIA Rennes-Bretagne Atlantique and Université Européenne de Bretagne
17 avenue de Cucillé, CS 64427, 35044 Rennes, France
romeo.tatsambon@cemagref.fr, christophe.collewet@cemagref.fr

ABSTRACT

This paper introduces a new approach for active fluid flows control: the vision-based approach. By using vision, dense flow velocity maps can be estimated and used in an observer-free closed-loop scheme to control a flow. This new approach is validated on a 2D plane Poiseuille flow and is proven to outperform the existing Poiseuille flow control appraches which use a limited number of available shear stress measurements.

1 INTRODUCTION

A significant part of the work carried out in the field of flows control has been dedicated to the control of the transition from laminar to turbulent states. Delaying, accelerating or modifying this transition can be of great environmental and economical interests for industrial applications. For instance, a drag reduction can be obtained while enhancing the lift, leading consequently to limit fuel consumption for aircrafts.

Flows control can be achieved in two different ways: passive or active control. Passive control provides a permanent action on a system. Most often it consists in optimizing shapes or in choosing suitable surfacing. Conversely, in active control an external energy is required to act on the system like, for example, techniques based on blowing and suction (Joshi et al. (1997)). This approach can be seen as an optimal problem where one has to apply an optimal control law based on a certain cost (minimization of the drag, minimization of the actuators power, etc.) (Bewley and Liu (1998)). However, very often, only open-loop control and forcing are used (Protas and Weisfred (2002)). As a matter of fact, designing a closed-loop control law requires the use of sensors that can be at the same time non-intrusive, accurate and adapted to the time and space scale of the phenomenon under monitoring. Unfortunately, such sensors are hardly available in the real context of control applications. The most commonly used measurement, obtained from MEMS, is the shear stress at a limited set of measurement points of the wall (Joshi et al. (1997)).

To deal with these issues, this paper proposes a vision-based control approach. As far as we know, such an approach has never been used for flows control issues. Vision-based control is now a well established technique in the robotics and automatic control communities. This technique has shown impressive results in numerous complex contexts such as underwater, medical and aeral robotic (Bonin-Font et al. (2008)). This technique consists in using feedback information provided by a vision sensor to control a dynamic system (Espiau et al. (1992)). By using vision, the complete flow can therefore be fully observed in real time (Champagnat et al. (2009)). This full observation is shown here to be of great improvements for flows control in comparison with existing control approaches that use only a limited set of walls shear stress observations (measurements).

In this paper we use the vision-based control approach to regulate the 2D plane Poiseuille flow around its steady state. In the next section we recall the modeling for the stabilization of this flow. In Section 3 we clearly define the unstable Poiseuille flow problem and we present the existing control solutions which include the Linear Quadratic Gaussian (LQG) regulator. The limitations of these solutions are clearly highlighted in the same section. In Section 4 the vision-based control approach is presented and theoretically proven to overcome the aformentioned limitations in Section 5. Since the LQG approach is the standard effective approach for flows control, In Section 6 we compare the vision-based and the LQG approaches. Simulations are given in Section 7 to validate the proposed approach.

2 MODELING OF 2D PLANE POISEUILLE FLOW FOR CONTROL

In this section we first present the basics of plane Poiseuille flow, then we recall the boundary control principle for this flow and finally we present the reduced linearized model used to derive the currently existing shear stress based control laws.

2.1 Basics

Fig. 1 illustrates the steady state velocities profile of the 2D plane Poiseuille flow where we can see that the x-direction is associated to the streamwise direction and the y-direction is associated to the normal direction. A 2D plane Poiseuille flow is a flow in a infinite length channel due to a pressure gradient. The non-dimensionalised Navier-Stokes equations (NSE) of this flow are given by
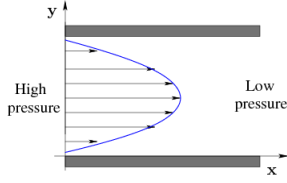
Figure 1. Steady state velocities profile of the 2D plane Poiseuille flow.

$$\begin{cases} \dfrac{\partial \mathbf{V}}{\partial t} + (\mathbf{V} \cdot \nabla)\mathbf{V} = -\nabla P + \dfrac{1}{R_e}\nabla^2 \mathbf{V} \\ \nabla \cdot \mathbf{V} = 0 \\ \mathbf{V}(x, y = \pm 1, t) = \mathbf{0} \end{cases} \quad (1)$$

where P is the pressure; $\mathbf{V}$ is the flow velocity; $\mathbf{V}(x, y = \pm 1, t) = \mathbf{0}$ represents the no slip boundary condition and R_e is the Reynolds number.

Since Poiseuille flow is simple, the analytical solution (V_{bx}, V_{by}, P_b) of (1) in the steady state case, i.e. $\frac{d\mathbf{V}}{dt} = \frac{\partial \mathbf{V}}{\partial t} + (\mathbf{V} \cdot \nabla)\mathbf{V} = \mathbf{0}$, can be found:

$$(V_{bx}, V_{by}, P_b) = (1 - y^2, 0, -\frac{2}{R_e}x). \quad (2)$$

This solution is illustrated on Fig. 1.

2.2 Control principle

A perturbed plane Poiseuille flow can be controlled via boundaries. Boundary control consists in modifying boundaries conditions as shown in (Joshi et al. (1997)).

From a physical point of view, boundary control can be interpreted as a geometric alteration of the boundary as pictured on Fig. 2. The boundary control on the upper and the lower channels can be theoretically modeled by functions χ_u and χ_l that ensure the mass conservation in the controlled system as pictured on Fig. 2. Note that in the absence of control, i.e. when $\chi_u = \chi_l = 0$, the red dashed curves (see Fig. 2) are aligned with the lower and upper boundary lines as expected.

2.3 Reduced order model of the unstable 2D plane Poiseuille flow

For a pratical implementation of flow control methods, the infinite dimension of a flow prompts the need of a reduced flow model. This section aims at deriving the reduced model of a controlled Poiseuille flow.

Concerning Poiseuille flow, most of the works focus on temporal instabilities caused by a perturbation velocity $\mathbf{V_p}(x, y, t)$. In order to keep permanent such instabilities in the infinite channel when the flow is not controlled, a periodic boundary finite length channel is assumed (Joshi et al. (1997)). That is why the perturbation velocity $\mathbf{V_p}(x, y, t)$ can be expanded in a Fourier series

$$\mathbf{V_p}(x, y, t) = \sum_{n=-\infty}^{+\infty} V_p^n(y, t)e^{i\alpha_n} \quad (3)$$

where $\alpha_n = n\alpha_0$, with $\alpha_0 = \frac{2\pi}{L_x}$ the fundamental wavenumber and L_x is the streamwise period length (see Fig. 2).

The modeling, required to derive shear stress based control laws, consists first of all in linearizing the NSE around the steady state solution (2). Then the continuous linearized
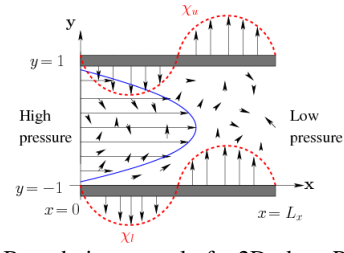

Figure 2. Boundaries control of a 2D plane Poiseuille flow, L_x is the streamwise channel length.

model of the NSE is reduced by approximation of the perturbation velocity $\mathbf{V_p}(x, y, t)$ at a specifically selected wavenumber α_n of the Fourier series (3); and by decomposition of the Fourier series coefficient $V_p^n(y, t)$ through the evaluation of combinations of Chebychev polynomials Φ_m at Gauss-Lobatto collocation points y_k as follows

$$V_p^n(y_k, t) = \sum_{m=1}^{M} p_m^n(t)\Phi_m(y_k) \text{ with } 1 \leq k \leq M. \quad (4)$$

Finally, the null boundary conditions of the closed-loop control system is obtained by setting the upper and lower boundaries to the values of the control inputs χ_u and χ_l respectively. The details of the derivation of the reduced linearized model are given in (McKernan (2006)).

All computation done, the reduced linearized model can be presented in the following canonical expression

$$\begin{cases} \dot{\mathbf{p}}^\mathbf{n}(t) = \mathbf{A^n}\mathbf{p^n}(t) + \mathbf{B^n}\mathbf{u}(t) \\ \mathbf{z}(t) = \mathbf{C}^{\top\mathbf{n}}\mathbf{p^n}(t) \\ \mathbf{p^n}(0) = \mathbf{p^n}_0 \end{cases} \quad (5)$$

where $\mathbf{p^n}(t) = (p_m^n)$ is the state vector, $\mathbf{A^n}$ is the state matrix, $\mathbf{u}(t) = (u_u(t), u_l(t))$ is the system control inputs on the upper and lower channel boundaries, $\mathbf{B^n}$ is the input matrix, $\mathbf{C^n}$ is the output matrix and $\mathbf{z}(t)$ is the vector of shear stress measurements on the upper and lower boundaries.

3 A classical problem and the existing solutions

In this section we present the unstable flow problem related to the 2D plane Poiseuille flow. Then we present existing control solutions based on shear stress measurements and we also highlight their main limitations.

3.1 Unstable flow

In the case where the Reynolds number is set to $Re = 10\,000$, the reduced linearized model (5) is unstable only for the wavenumber $\alpha_n = 1$ (Orszag (1971)). This instability can be seen through the poles of the state matrix $\mathbf{A^n}$. These poles are illustrated on Fig. 3, where we can see the unstable mode $\lambda = 0.00373967 \pm i0.23752649$. Note that a mode is a complex conjugate pair of eigenvalues. In this case the flow is initially in the steady state but in an unstable equilibrium, i.e. a small disturbance velocity value $\mathbf{V_p}(x, y, t)$ destabilizes the uncontrolled fluid flow.

3.2 Existing control solutions

Using the classical output feedback control $\mathbf{u}(t) = -\alpha z(t)$ in (5) with α a scalar gain $z(t)$ is a single shear stress measurement, the unstable 2D Poiseuille
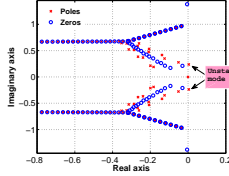
Figure 3. Poles and zeros of the reduced linearized system for $Re = 10\,000$, $\alpha_n = 1$.

flow can be stabilized as shown in (Joshi et al. (1997)). However this simple proportional controller generally fails to suppress unobservable high transient modes which could trigger transition to turbulence as explained in (Joshi et al. (1997)). By assuming the availability of the value of the state vector $\mathbf{p^n}(t)$, a state feedback Linear Quadradic Regulator (LQR), can easily stabilize the unstable pertubed Poseuille flow (Bewley and Liu (1998), McKernan (2006)). However, in practice the LQR approach can not be used since it requires the unknown value of the true state value $\mathbf{p^n}(t)$. That is why the output feedback LQG regulation is generally considered as an effective approach for flow control issues (Bewley and Liu (1998), McKernan (2006)). This approach uses an estimated value $\widehat{\mathbf{p^n}}(t)$ of the state vector: the value of $\widehat{\mathbf{p^n}}(t)$ is obtained from the shear stress measurements $\mathbf{z}(t)$ using an observer built from a Linear Quadratic Estimation (LQE) scheme. The control signal for the output feedback LQG regulator is thus given by

$$\mathbf{u}(t) = -\mathbf{k}^\top \widehat{\mathbf{p^n}}(\mathbf{z}(t)), \qquad (6)$$

where vector $\mathbf{k}$ is the LQR optimal gain. We recall that the LQR signal minimizes the following cost function

$$\int_0^\infty \left(\mathbf{p^{n'}}(t) \mathbf{Q} \mathbf{p^n}(t) + \mathbf{u}'(t) \mathbf{R} \mathbf{u}(t) \right) \mathrm{d}t \qquad (7)$$

where $\mathbf{Q}$ and $\mathbf{R}$ are positive semidefinite weighting matrices. Matrix $\mathbf{Q}$ is used to limit the kinetic energy density $\mathscr{E}_n(t) = \mathbf{p^{n'}}(t) \mathbf{Q} \mathbf{p^n}(t)$ developed in (McKernan (2006)). Matrix $\mathbf{R}$ is used to limit energy comsumption by actuators. In order to maintain wall symmetry, matrix $\mathbf{R}$ is set as a scaled identity matrix (McKernan (2006)), i.e. $\mathbf{R} = r^2 \mathbf{I}$, where r is a real positive parameter. This last control law will be refer to as shear stress based LQG (SSB-LQG) control.

The observer used by the SSB-LQG control suffers from the initialization issue as we will show in Section 6.1. In addition in the case where the limited shear stress measurements $\mathbf{z}(t)$ are noisy, the estimate $\widehat{\mathbf{p^n}}(t)$ is also noisy. Both of these problems are solved the proposed vision-based control approach, which is introduced in the next section.

4 FUNDAMENTALS OF VISION-BASED CONTROL

To achieve a closed-loop vision-based control task, a set of visual features $\mathbf{s}(t)$ is selected from the image of the scene. Indeed, only a part of the image (provided by the sensor) is used to define a diffeomorphic map between the observed scene and a judiciously selected set of features in the image. A control law is then designed so that the visual features $\mathbf{s}(t)$ reaches a desired value $\mathbf{s}^*$ corresponding to a desired state of the system. The control principle is thus to regulate the error vector $\mathbf{e}(t) = \mathbf{s}(t) - \mathbf{s}^*$ to zero.

To design the control law, the dynamic of the error vector must be known. This dynamic is given by

$$\dot{\mathbf{e}}(t) = \frac{\partial \mathbf{e}(t)}{\partial t} + \mathbf{L_e}(t) \mathbf{u}(t), \qquad (8)$$

where $\mathbf{u}(t)$ is the system control inputs, $\mathbf{L_e}(t)$ is the jacobian matrix that encodes the time variation of the visual features with respect to the variation of the control signal acting on the system (Espiau et al. (1992)), and $\partial \mathbf{e}(t)/\partial t$ expresses the variation of the error vector due to the free motion of the visual features.

A key point in vision-based control is that this control technique belongs to the class of sensor-based control of dynamic systems: the control law is computed in the sensor frame (Samson et al. (1991)). Consequently, this approach corresponds clearly to an observer-free feedback control. In the following we apply the vision-based approach to the regulation of plane Poiseuille flow.

5 VISION-BASED CONTROL OF FLOWS

In the particular case of flows control, a control law is designed from visual features obtained from the vision system sensing the flow. Of course a great advantage of such a sensor is that it is non-intrusive. This sensor is also an extremely rich and dense source of information on the flow. Indeed a large spectrum of visual features $\mathbf{s}(t)$ could be selected from the image, such as coordinates of singular points in the flow or the vorticity map. Nevertheless, to directly compare our vision-based approach to the SSB-LQG approach we choose the same data, i.e. $\mathbf{s}(t) = \widehat{\mathbf{p^n}}(t)$. However, as shown in the next section, the main difference between both approaches is the way to estimate $\widehat{\mathbf{p^n}(t)}$. We first show in our approach how $\widehat{\mathbf{p^n}(t)}$ is estimated from visual measurements, and then we present the control law.

5.1 Visual sensing of flows

A laser sheet is used to enlighten the particles for which the velocity has to be computed (see Fig. 4). Consequently, from this visualization process, it is possible to compute dense flow velocity maps from optical flow techniques. Optical flow can be defined as the apparent velocity vector field representing the motion of photometric pattern (pixels brightness) in successive image sequences (Heitz et al. (2010)). We first present the perspective projection of a flow particle, then we show how to estimate a flow particle velocity from its image velocity, and finally we present the computation of the state vector from the velocity of a fow particle.

5.1.1 Perspective projection of a flow particle:

Let $^o\mathbf{M} = (^oM_x(t), {}^oM_y(t), {}^oM_z(t))$ be the space-time coordinates of the flow particle $\mathscr{M}$ (see Fig. 5) expressed in the flow frame $\mathscr{F}_o$. The perspective projection of $\mathscr{M}$ is obtained in three steps.

• The first step consists to express $\mathscr{M}$ in the camera frame. Let $^c\mathbf{M} = (^cM_x(t), {}^cM_y(t), {}^cM_z(t))$ be the space-time coordinates of $\mathscr{M}$ expressed in the camera frame $\mathscr{F}_c$. The relationship between $^c\mathbf{M}(t)$ and $^o\mathbf{M}(t)$ is given by

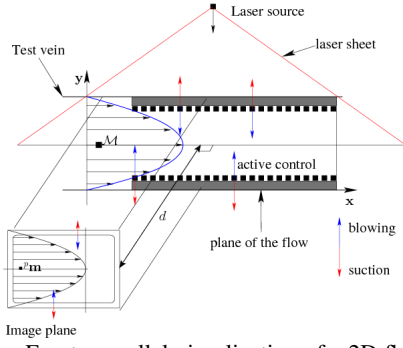$$^c\mathbf{M}(t) = {}^c\mathbf{R}_o {}^o\mathbf{M}(t) + {}^c\mathbf{t}_o \qquad (9)$$

3

Figure 4. Fronto-parallel visualization of a 2D flow using a laser sheet which role is to enlighten the particles seeded in the fluid: $^p\mathbf{m}$ is the perspective image of the fluid particle $\mathcal{M}$.
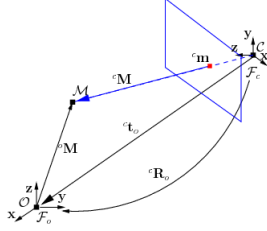

Figure 5. Perspective projection of a flow particle.

where $(^c\mathbf{R}_o, {}^c\mathbf{t}_o)$ is the rigid constant kinematic link between the camera and the flow frames (see Fig. 5). This rigid link is also known as extrinsic camera parameters.

- In the second step, the perspective projection $^c\mathbf{m}(t) = (^cm_x(t), {}^cm_y(t))$ of point $^c\mathbf{M}(t)$ obtained from the well-known pinhole camera model is given by:

$$^cm_x(t) = \frac{^cM_x(t)}{^cM_z(t)}, \; {}^cm_y(t) = \frac{^cM_y(t)}{^cM_z(t)}. \tag{10}$$

- Finally in the last step the perspective coordinates vector $^c\mathbf{m}(t)$ is expressed in the sensor space (i.e. in pixel unit) as $^p\mathbf{m}(t) = (^pm_x(t), {}^pm_y(t))$, by the relation

$$^pm_x(t) = \frac{f}{l_x}{}^cm_x(t) + u_0, \; {}^pm_y(t) = \frac{f}{l_y}{}^cm_y(t) + v_0 \tag{11}$$

where l_x (respectively l_y) is the pixel size (in meter) in the x (respectively) y direction, f is the focal length and (u_0, v_0) is the vector coordinates of the principal point of the camera. Note that vector $(f_x = f/l_x, f_x = f/l_x, u_0, v_0)$ represents the intrinsic camera parameters. Both the intrinsic and the extrinsic camera parameters can be determined using the calibration method described in (Tsai (1987)).

5.1.2 Estimation of the flow velocity particle from its image velocity:

Now we show in three steps how to compute the velocity of a flow particle $\mathcal{M}$ from its perspective image $^p\mathbf{m}$. The first step consists in expressing the relationship between the flow particle and its perspective image velocities. From (11), it is easy to show that the relationship between the image velocities $^p\dot{\mathbf{m}}$ and the flow velocities $^o\dot{\mathbf{M}}(t) = \begin{bmatrix} ^o\dot{M}_x(t) & ^o\dot{M}_y(t) & ^o\dot{M}_z(t) \end{bmatrix}^\top$ is given by

$$^p\dot{\mathbf{m}}(t) = \frac{\partial^p\mathbf{m}}{\partial^c\mathbf{M}}{}^c\mathbf{R}_o{}^o\dot{\mathbf{M}} \tag{12}$$

where the jacobian matrix $\frac{\partial^p\mathbf{m}}{\partial^c\mathbf{M}}$ is given by

$$\frac{\partial^c\mathbf{m}}{\partial^c\mathbf{M}} = \begin{bmatrix} \frac{f_u}{M_z(t)} & 0 & -\frac{f_u M_x(t)}{M_z^2(t)} \\ 0 & \frac{f_v}{M_z(t)} & -\frac{f_v M_y(t)}{M_z^2(t)} \end{bmatrix}. \tag{13}$$

In the 2D case, since $^oM_z(t)$ is constant, we have $^o\dot{M}_z(t) = 0$ and (12) can be rewritten as

$$\begin{bmatrix} ^p\dot{m}_x(t) \\ ^p\dot{m}_y(t) \end{bmatrix} = \frac{\partial^p\mathbf{m}}{\partial^c\mathbf{M}}{}^c\mathbf{R}_o|_{12} \begin{bmatrix} ^o\dot{M}_x(t) \\ ^o\dot{M}_y(t) \end{bmatrix} \tag{14}$$

where $\mathbf{R}_o|_{12}$ is the restriction of the orientation matrix $^c\mathbf{R}_o$ to its two first columns.

The second step consists to estimate the image velocity $^p\dot{\mathbf{m}}$. This estimation can be done using optical flow techniques (Heitz et al. (2010)). In brief, this technique exploits the brightness conservation equation at pixel $^p\mathbf{m}(t)$ as follows

$$0 = \frac{dI_m(t)}{dt} = \frac{\partial I_m(t)}{\partial t} + \nabla I_m^\top {}^p\dot{\mathbf{m}}, \tag{15}$$

where $I_m(t)$ is the brightness of pixel $^p\mathbf{m}(t)$ and ∇I_m is the brightness spatial gradient. There are many methods which can be used to compute $^p\dot{\mathbf{m}}(t)$. All of these methods use the assumption that $^p\dot{\mathbf{m}}$ is also the image velocities of all the pixels in the local neighbourhood of pixel $^p\mathbf{m}(t)$. The most advanced methods take also into account an a priori information such as a local parametric motion model. A comprehensive review of some NSE consistent optical flow methods is available in (Heitz et al. (2010)).

Finally, assuming a perfectly calibrated camera, the flow perturbation velocities $\widehat{\mathbf{V}_\mathbf{p}}(x, y, t)$ can be computed from optical flow measurements by inverting (14).

5.1.3 Estimation of the state vector:

This last step shows how to compute $\widehat{\mathbf{p}^\mathbf{n}}(t)$ from the estimation $\widehat{\mathbf{V}_\mathbf{p}}(x, y, t)$. This is simply done by projecting the perturbation velocities $\widehat{\mathbf{V}_\mathbf{p}}(x, y, t)$ onto Fourier and Chebychev bases. Due to a lack of space, the details of this projection are omitted in this paper.

It is worth mentioning that an important contribution of our vision-based state estimation method is the fact that the initial value $\widehat{\mathbf{p}^\mathbf{n}}(t = 0)$ is no longer of concerned in our approach as shown in Section 6.2. In addition, because of dense flow velocity maps, the vision-based approach provides less noisy estimations of the state vector as shown also in Section 6.2.

5.2 Closed-loop vision-based control of flows

As mentioned at the very begining of Section 5, we choose the same data $\mathbf{s}(t) = \widehat{\mathbf{p}^\mathbf{n}}(t)$ as in the SSB-LQG approach so that our vision-based approach can be directly compare to the SSB-LQG approach. In that case, it becomes easy to express the dynamic of the error of the visual features $\mathbf{e}(t)$ (see (8)) around the steady state solution (the equilibrium point). In the ideal case where there is no state disturbances and there is no image noise, from the ideal state dynamic equation given in (5), it is straightforward that the ideal image error dynamic given by (8) is such that

$$\frac{\partial\mathbf{e}(t)}{\partial t} = \mathbf{A}^\mathbf{n}\mathbf{e}(t), \; \mathbf{L}_\mathbf{e}(t) = \mathbf{B}^\mathbf{n} \text{ with } \mathbf{e}(t) = \mathbf{p}^\mathbf{n}(t). \tag{16}$$

More precisely (16) can be interpreted as follows: the term $\frac{\partial\mathbf{e}(t)}{\partial t}$ describes the instationary aspect of the flow image velocity map due to the motion of the uncontrolled flow, and

the term $\mathbf{L_e}(t)$ encodes the spatial inhomogeneity aspect of the flow image velocity map due to unsteady actuation (for instance blowing and suction actions). Therefore, around the desired state, (8) can be rewritten as

$$\dot{\mathbf{p}}^{\mathbf{n}}(t) = \mathbf{A}^{\mathbf{n}}\mathbf{p}^{\mathbf{n}}(t) + \mathbf{B}^{\mathbf{n}}\mathbf{u}(t) \qquad (17)$$

and the simple state-feedback control law

$$\mathbf{u}(t) = -\mathbf{k}^\top \widehat{\mathbf{p}^{\mathbf{n}}}(t), \qquad (18)$$

can be used. We will refer to this vision-based control law as the vision-based LQG (VB-LQG) control law since $\widehat{\mathbf{p}^{\mathbf{n}}}(t)$ is obtained from visual measurements $^{p}\dot{\mathbf{m}}(t)$ instead of shear stress measurements as used in (6). In the next section, we compare the SSB-LQG approach with the proposed VB-LQG method.

6 COMPARISON BETWEEN THE SSB-LQG AND THE VB-LQG APPROACHES

The major difference between the SSB-LQG and the VB-LQG approaches is the estimation of the state vector $\widehat{\mathbf{p}^{\mathbf{n}}}(t)$: the SSB-LQG regulator uses an observer built from the LQE approach whereas the VB-LQG approach relies on an observer-free estimation method. We now highlight the influence of these estimation methods on the closed-loop system.

6.1 Closed-loop system with the SSB-LQG control

In the LQE framework it is supposed that the reduced linearized system (5) has process disturbances $\varepsilon_{\mathbf{p}}$ and measurements noise ε_z which are uncorrelated white Gaussian noise. The estimation error dynamic is given by

$$\begin{cases} \dot{\widehat{\mathbf{p}^{\mathbf{n}}}}(t) - \dot{\mathbf{p}}^{\mathbf{n}}(t) = (\mathbf{A}^{\mathbf{n}} - \mathbf{L}\mathbf{C}^{\mathbf{n}\top})(\widehat{\mathbf{p}^{\mathbf{n}}}(t) - \mathbf{p}^{\mathbf{n}}(t)) + \mathbf{L}\varepsilon_z(t) - \varepsilon_{\mathbf{p}}(t) \\ \widehat{\mathbf{p}^{\mathbf{n}}}(0) - \mathbf{p}^{\mathbf{n}}(0) = \mathbf{unknown}, \end{cases}$$

$$(19)$$

where $\mathbf{L}$ is the estimator optimal gain. The resulting closed-loop system is given by (McKernan (2006)):

$$\begin{cases} \begin{bmatrix} \dot{\mathbf{p}}^{\mathbf{n}}(t) \\ \dot{\widehat{\mathbf{p}^{\mathbf{n}}}}(t) - \dot{\mathbf{p}}^{\mathbf{n}}(t) \end{bmatrix} = \mathbf{M}_{lqg} \begin{bmatrix} \mathbf{p}^{\mathbf{n}}(t) \\ \widehat{\mathbf{p}^{\mathbf{n}}}(t) - \mathbf{p}^{\mathbf{n}}(t) \end{bmatrix} + \mathbf{M}_n \begin{bmatrix} \varepsilon_{\mathbf{p}}(t) \\ \varepsilon_z(t) \end{bmatrix} \\ \widehat{\mathbf{p}^{\mathbf{n}}}(0) - \mathbf{p}^{\mathbf{n}}(0) = \mathbf{unknown}. \end{cases}$$

$$(20)$$

where $\mathbf{M}_{lqg} = \begin{bmatrix} \mathbf{A}^{\mathbf{n}} - \mathbf{B}^{\mathbf{n}}\mathbf{k}^\top & -\mathbf{B}^{\mathbf{n}}\mathbf{k}^\top \\ \mathbf{0} & \mathbf{A}^{\mathbf{n}} - \mathbf{L}\mathbf{C}^{\top\mathbf{n}} \end{bmatrix}$, $\mathbf{M}_n = \begin{bmatrix} \mathbf{I} & \mathbf{0} \\ -\mathbf{I} & \mathbf{L} \end{bmatrix}$ with $\mathbf{I}$ an identity matrix. Equation (20) clearly shows that the true state dynamic $\dot{\mathbf{p}}^{\mathbf{n}}(t)$ (around the desired state) depends on the estimation error $\widehat{\mathbf{p}^{\mathbf{n}}}(t) - \mathbf{p}^{\mathbf{n}}(t)$. Therefore, since this error highly depends on the initial unknown estimation error $\widehat{\mathbf{p}^{\mathbf{n}}}(0) - \mathbf{p}^{\mathbf{n}}(0)$, a poor initialization of the observer could cause drive the system to a turbulent state as shown in McKernan (2006). In addition the noise in the measurements propagates in the control law (6), this is not suitable at all for the lifetime of the actuators.

6.2 Closed-loop system with the VB-LQG control

We first present the estimation of the state vector $\widehat{\mathbf{p}^{\mathbf{n}}}(t)$ in the case of noisy optical flow measurements and then we show system closed by the VB-LQG control. Let $\mathbf{V_p}(x,y,t)$ be the $M \times N$ pixels size image of the perturbation velocity map obtained from noise-free optical flow measurements. From (14), in the practical case where optical flow measurements $^{p}\dot{\mathbf{m}}$ are corrupted by a Gaussian noise process, the computed flow perturbation velocities $\mathbf{V_p}$ are also affected by Gaussian noise. Without lost of generality the noisy perturbation velocity map can be written as $\widehat{\mathbf{V_p}}(x,y,t) = \mathbf{V_p}(x,y,t) + \varepsilon(x,y,t)$. This noisy pertubation velocity map $\widehat{\mathbf{V_p}}(x,y,t)$ is used to compute the estimation of the state vector $\mathbf{p}^{\mathbf{n}}(t)$ as shown in (Tatsambon Fomena and Collewet (2011)):

$$\widehat{\mathbf{p}^{\mathbf{n}}}(t) = \mathbf{p}^{\mathbf{n}}(t) + \frac{1}{N}\mathbf{e}^{\mathbf{n}}(t), \qquad (21)$$

where vector $\mathbf{e}^{\mathbf{n}}(t)$ the projection of the measurements noise matrix $\varepsilon(x,y,t)$ onto Fourier and Chebychev basis.

The resulting vision-based closed-loop system, obtained from (5) and (21), is given by

$$\begin{cases} \dot{\mathbf{p}}^{\mathbf{n}}(t) = \mathbf{A}^{\mathbf{n}}\mathbf{p}^{\mathbf{n}}(t) + \mathbf{B}^{\mathbf{n}}\mathbf{u}(t) \\ \mathbf{u}(t) = -\mathbf{k}^\top \widehat{\mathbf{p}^{\mathbf{n}}}(t) \\ \widehat{\mathbf{p}^{\mathbf{n}}}(t) = \mathbf{p}^{\mathbf{n}}(t) + \frac{1}{N}\mathbf{e}^{\mathbf{n}}(t), \end{cases} \qquad (22)$$

where $\mathbf{k}$ is the LQR optimal gain. The closed-loop reduced linearized system (22) can be rewritten as

$$\dot{\mathbf{p}}^{\mathbf{n}}(t) = (\mathbf{A}^{\mathbf{n}} - \mathbf{B}^{\mathbf{n}}\mathbf{k}^\top)\mathbf{p}^{\mathbf{n}}(t) - \frac{1}{N}\mathbf{B}^{\mathbf{n}}\mathbf{k}^\top\mathbf{e}^{\mathbf{n}}(t). \qquad (23)$$

The initial value $\widehat{\mathbf{p}^{\mathbf{n}}}(t=0)$ is therefore no longer of concerned in our approach. In addition for a large number of points N in the streamwise direction (typically N=1024 for a standard image), the reduced linearized system dynamic equation (23) is less affected by measurements noise since $\frac{1}{N}\mathbf{B}^{\mathbf{n}}\mathbf{k}^\top\mathbf{e}^{\mathbf{n}}(t)$ tends to $\mathbf{0}$. This is another great improvement over the SSB-LQG control scheme that is always noise dependent when noisy shear stress values are used in the LQE as shown in (20).

7 RESULTS

Validations of our approach is done using synthetic data sets of spatio-temporal variations of the perturbation velocities $\mathbf{V_p}(x,y,t)$ obtained from the Poiseuille flow reduced model presented in (5). This reduced model is used to build a linear simulator of 2D channel Poiseuille flow with the following classical characteristics as used in related works (Joshi et al. (1997), Bewley and Liu (1998), McKernan (2006)): $R_e = 10\,000$, $L_x = 4\pi$ and $\alpha_n = 1$. Matrices $\mathbf{A}$, $\mathbf{B}$, $\mathbf{C}$ given in (5) have been computed for $M = 250$ using Matlab codes provided in (McKernan (2006)).

7.1 Comparison of the state estimations

Results are given in Fig. 6. Fig. 6(a) presents the ideal case where we can see that both estimations perfectly correspond to the ground truth value of the state vector. Fig. 6(b) highlights the initialization and the asymptotic convergence issues in the LQE; these issues are not of concerned in the vision-based approach which provides the ground truth value of the state vector. In order to show the robustness to noise of the vision-based approach, the standard deviation (STD) on the optical flow noise has been purposely set to a value 10 times higher than the STD on the shear stress noise. As shown on Fig.6(c), due to a large number of flow velocities provided by the optical flow, the new approach is robust to noisy measurements.
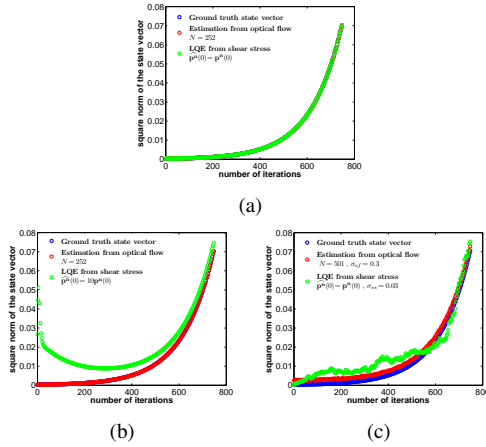
(a)

(b)   (c)

Figure 6.   Comparison of state vector estimations using shear stress and optical flow: (a) ideal case, (b) LQE poor initialization, (c) measurements noise with a large number of pixels N.

(a)   (b)

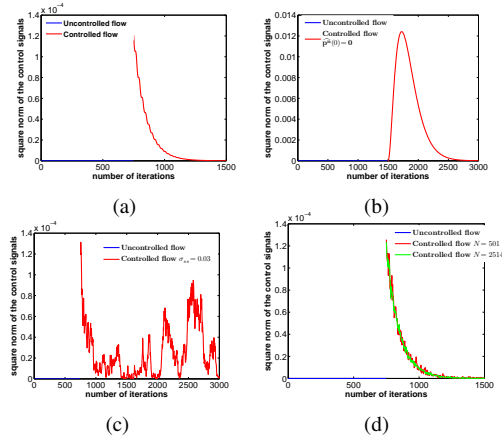(c)   (d)

Figure 7.   Comparison of SSB-LQG and VB-LQG controls: (a) ideal case, (b) initialization error in the SSB-LQG, (c) measurements noise in the SSB-LQG, (d) measurements noise in the VB-LQG.

7.2   Comparison of the behavior of the closed-loop systems

Results are presented in Fig. 7. Fig. 7(a) depicts the behavior of the control signal in the ideal case (no measurements noise, no initialization error). Fig. 7(b) depicts the behavior of the control signal when the initial value is set as $\widehat{\mathbf{p^n}}(0) = \mathbf{0}$ by default since the value of $\widehat{\mathbf{p^n}}(0)$ is unknown. In this case we can see that the value of the control signal can be 100 times higher than the ideal control signal case which includes the LQG-VB approach (compare the highest control signal values in Fig.7(b) and 7(a)). This higher control signal value could lead to an unsuitable state trajectory which can cause the real non-linear system to diverge as shown in (McKernan (2006)). In addition, as expected, the control signal (see Fig. 7(b)) takes more time to converge to 0 (3000 iterations compared to the VB-LQG approach). This leads to an energy consumption far much higher for the SSB-LQG control than for the VB-LQG control. The figures on the second row present the measurements noise case. Fig. 7(c) pictures the case of the SSB-LQG control, where we can see that the control signal does not converge to 0. Although the noise STD has been set to a small value, $\sigma_{ss} = 0.03$, the control signal is very noisy, which is not

suitable for actuators. Finally, Fig. 7(d) illustrates the robustness of the vision-based control where the STD in the optical flow noise is 10 times higher than the STD in the shear stress noise: we can see from this last figure that the control converges, and we can also see that the larger the sample of flow velocities used the lesser the noise in the control signal.

8   CONCLUSION

In this paper we have proposed a vision-based approach for fluid flow estimation and control which builds on optical flow techniques, which is non-intrusive, robust to measurements noise and suitable for fluid flows control. Theoretical proofs have been given in order to validate the improvements provided by the vision-based approach over the shear stress based LQG control in terms of the state vector estimation and flows control. Simulation results have been presented to validate the proposed approach. Future works will focus on the extension of the vision-based approach to the control of 3D flows.

REFERENCES

T. Bewley and S. Liu. Optimal and robust control and estimation of linear paths to transition. *J. Fluid Mech.*, 365: 305–349, 1998.

F. Bonin-Font, A. Ortiz, and G. Oliver. Visual navigation for mobile robots: a survey. *Journal of Intelligent & Robotic Systems*, 53(3):263–296, 2008.

F. Champagnat, A. Plyer, G. Le Besnerais, B. Leclaire, and Y. Le Sant. How to calculate dense piv vector fields at video rate. In *8th Int. Symp. On Particle Image Velocimetry*, Melbourne, Victoria (Australia), Aug. 2009.

B. Espiau, F. Chaumette, and P. Rives. A new approach to visual servoing in robotics. *IEEE Trans. on Robotics and Automation*, 8(3):313–326, June 1992.

D. Heitz, E. Mémin, and C. Schnörr. Variational fluid flow measurements from image sequences: synopsis and perspectives. *Exp. Fluids*, 48(3):369–393, 2010.

S. Joshi, J. Speyer, and J. Kim. A systems theory approach to the feedback stabilization on infinitesimal and finite amplitude disturbances in plane Poiseuille flow. *J. Fluid Mech.*, 332:157–184, 1997.

J. McKernan. *Control of plane Poiseuille flow: a theoretical and computational investigation*. PhD thesis, Cranfield University, 2006.

S. Orszag. Accurate solution of the Orr-Sommerfeld stability equation. *J. Fluid Mech.*, 50:689–703, 1971.

B. Protas and J. Weisfred. Drag force in the open-loop control of the cylinder wake in the laminar regime. *Physics of Fluids*, 14(2):810–826, 2002.

C. Samson, M. Le Borgne, and B. Espiau. *Robot control: the Task Function approach*. Oxford University Press, 1991.

R. Tatsambon Fomena and C. Collewet. Fluid flows control using visual servoing. In *18th IFAC World Congress*, Milan, Italy, 2011.

R.Y. Tsai. A versatile camera calibration technique for high-accuracy 3D machine vision metrology using off-the-shelf tv cameras and lenses. *IEEE Journal of Robotics and Automation*, 3(4):323–344, Aug 1987.